Supplementary Information

Hollow-needle-like nanocarbon with inner wall discriminating chirality

Jun Maruyama,* Shohei Maruyama, Tsutomu Shinagawa, Yuko Takao, Akira Takatsuki, Noriko Yoshizawa, Masataka Inoue, Natsuki Imai, Koichi Matsuo, Fumito Tani, Hirotomo Nishihara, Hideki Tanaka

Decomposition of tetrakis(4-ethynylphenyl)methane

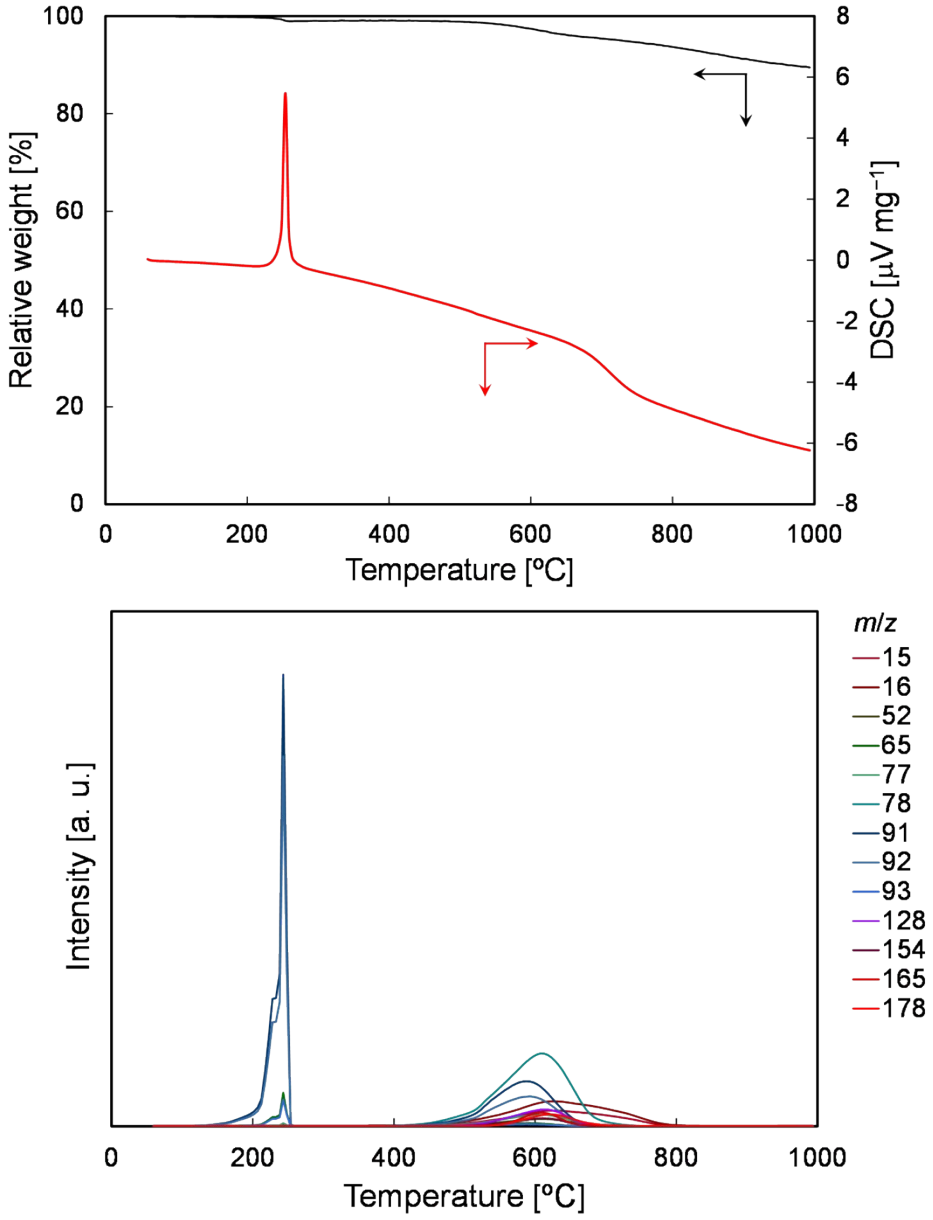

Figure S1. TG-DSC-MS profiles of tetrakis(4-ethynylphenyl)methane.

Decomposition of (*R*)-BINOL

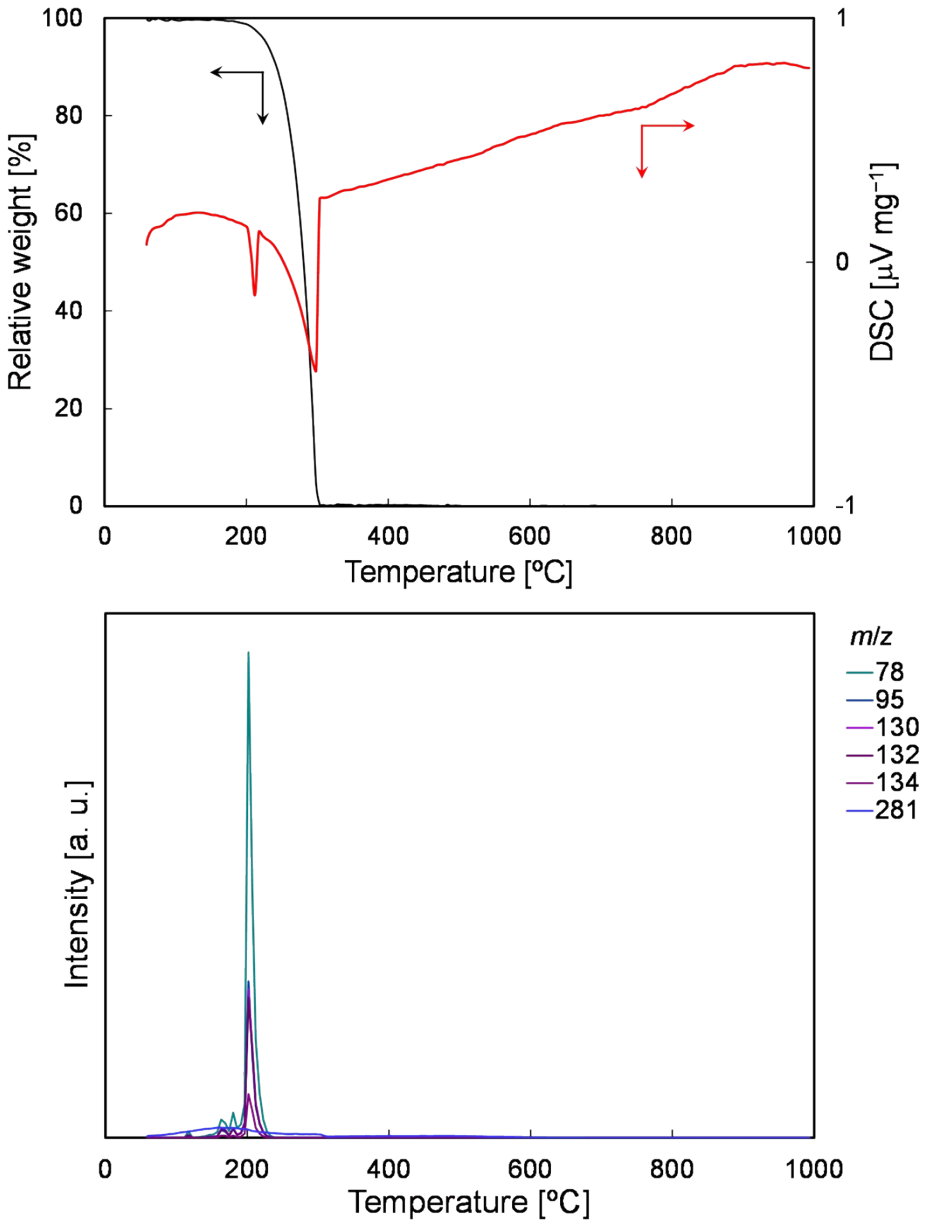

Figure S2. TG-DSC-MS profiles of (*R*)-BINOL.

Decomposition of (*S*)-BINOL

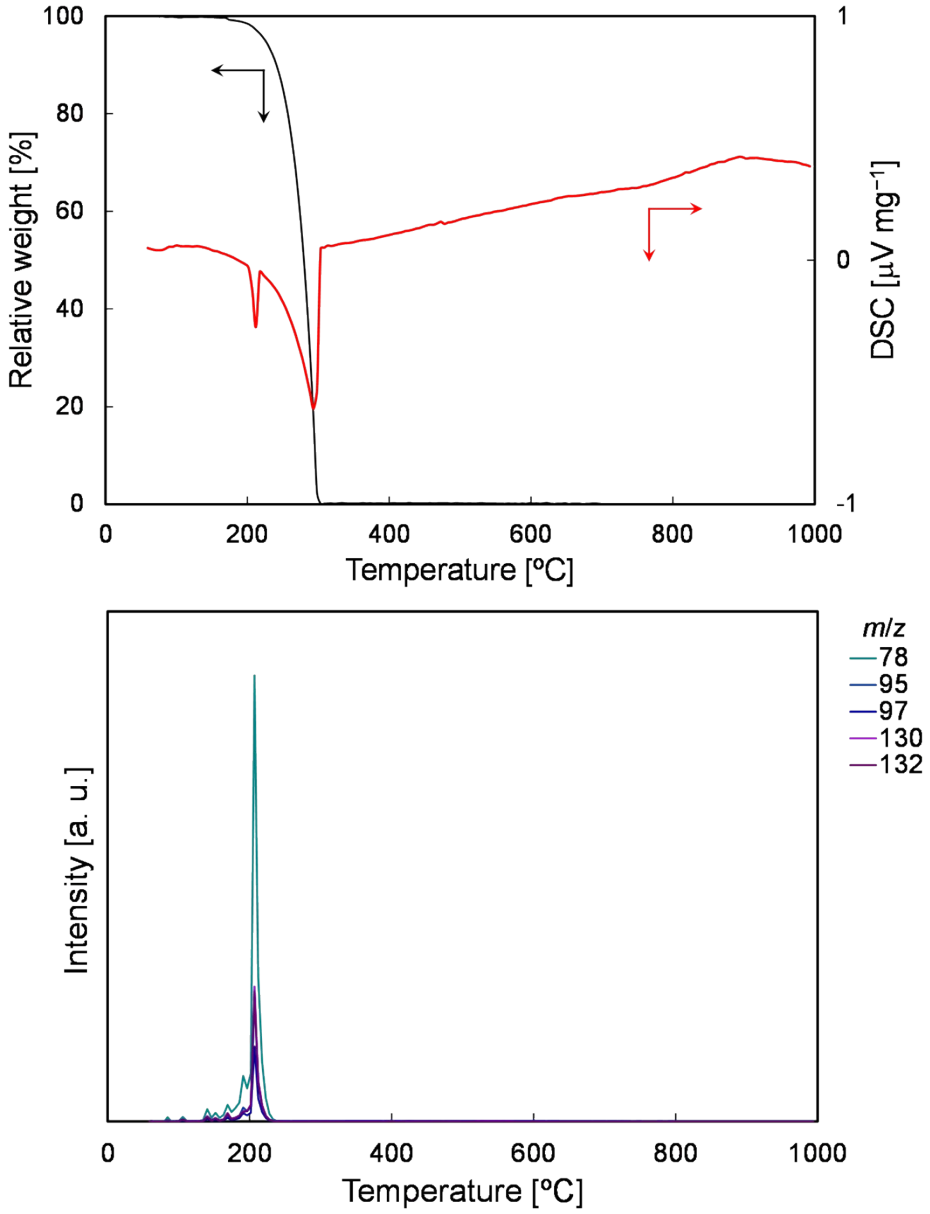

Figure S3. TG-DSC-MS profiles of (*S*)-BINOL.

Sublimation of C_{60}

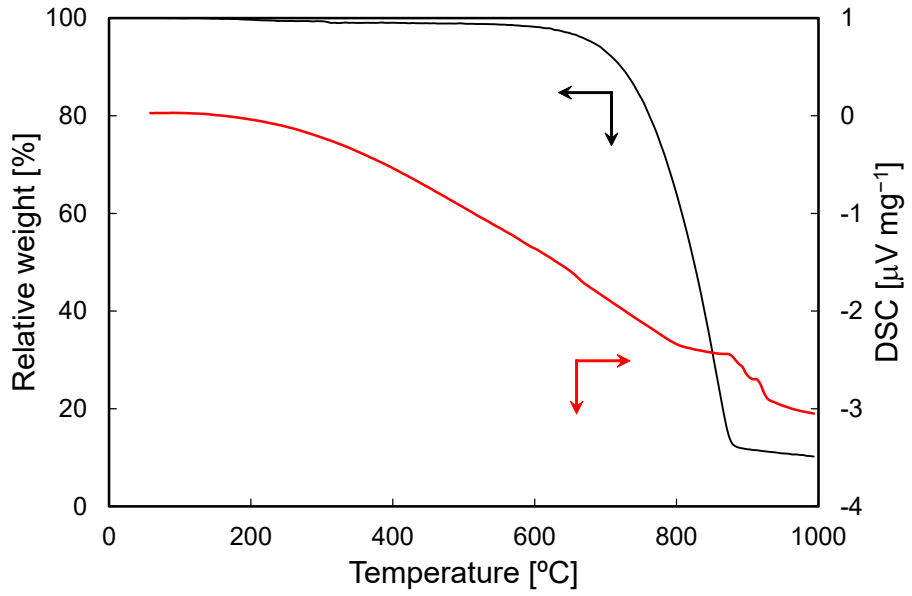

Figure S4. TG-DSC profiles of C_{60}. The MS profile is omitted because of the deposition of the sublimed C_{60} between TG and MS.

Decomposition of T*R*

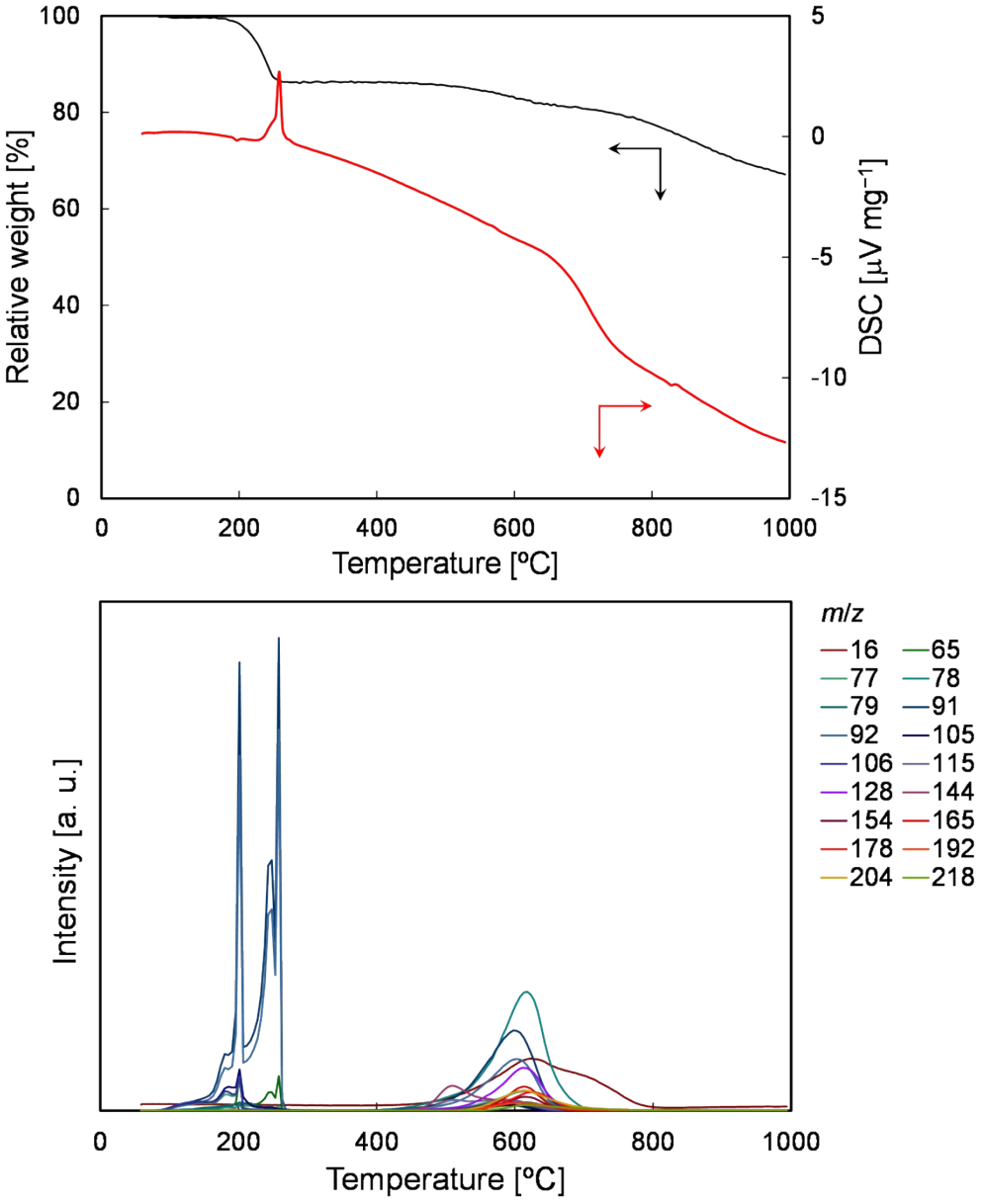

Figure S5. TG-DSC-MS profiles of T*R*.

Decomposition of T*S*

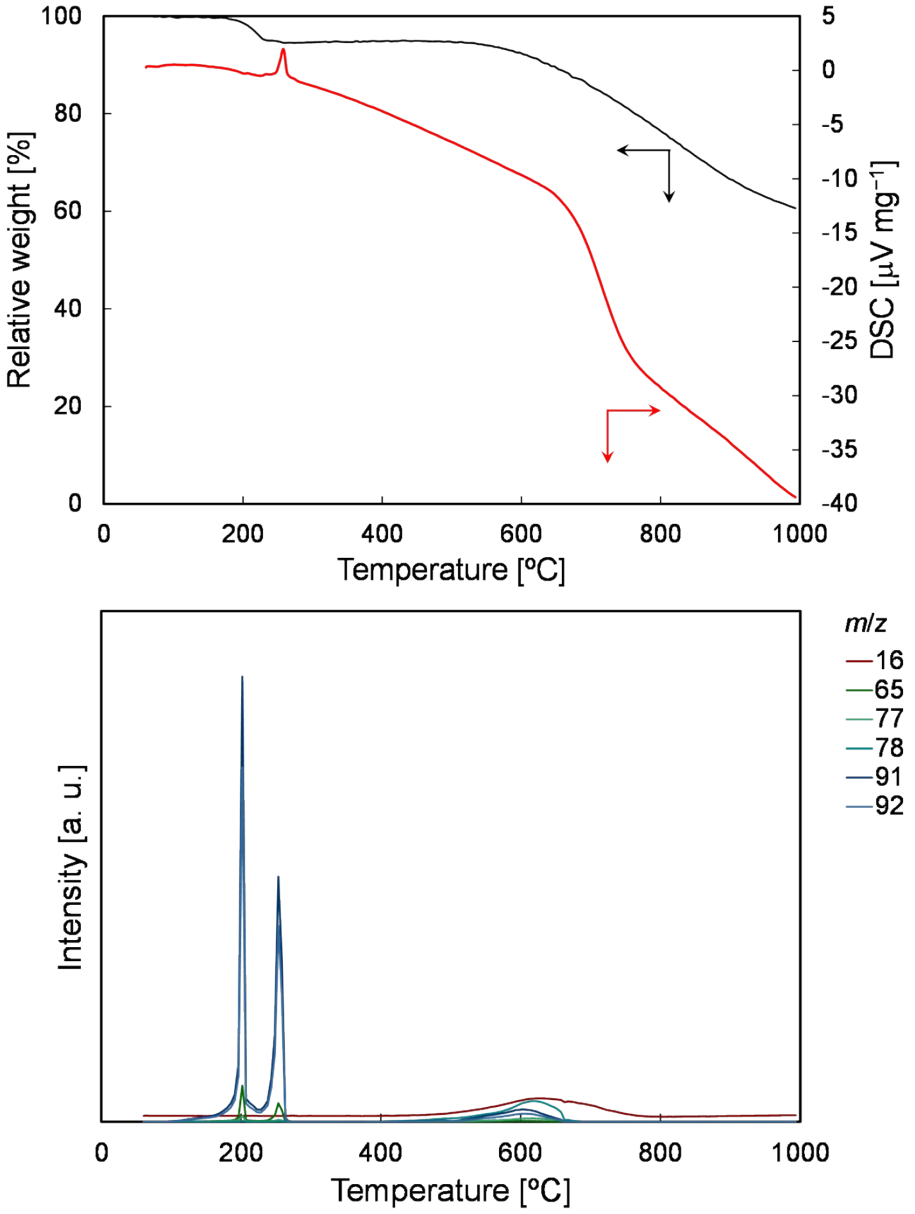

Figure S6. TG-DSC-MS profiles of T*S*.

Decomposition of TF

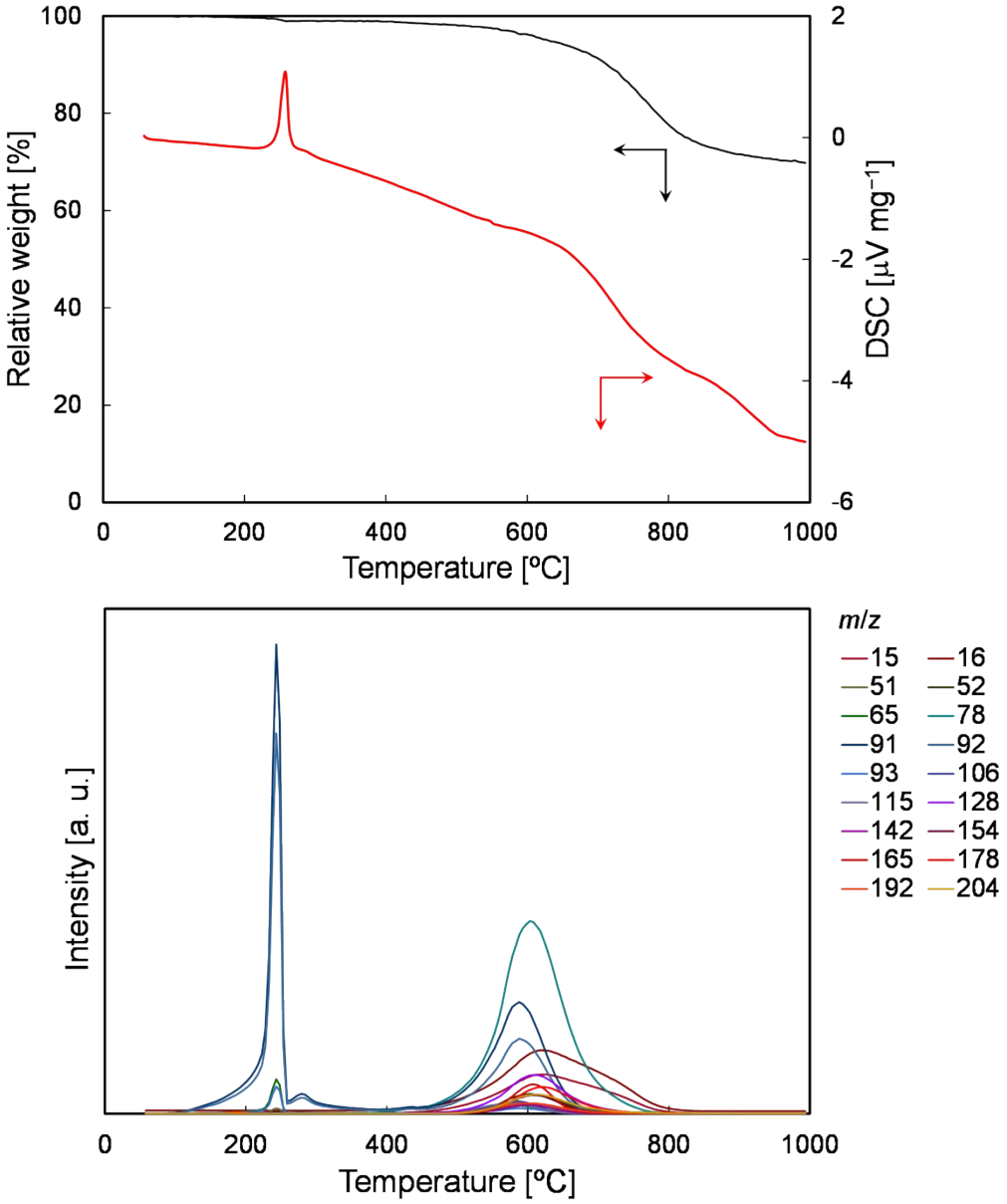

Figure S7. TG-DSC-MS profiles of TF.

Decomposition of TF*R*

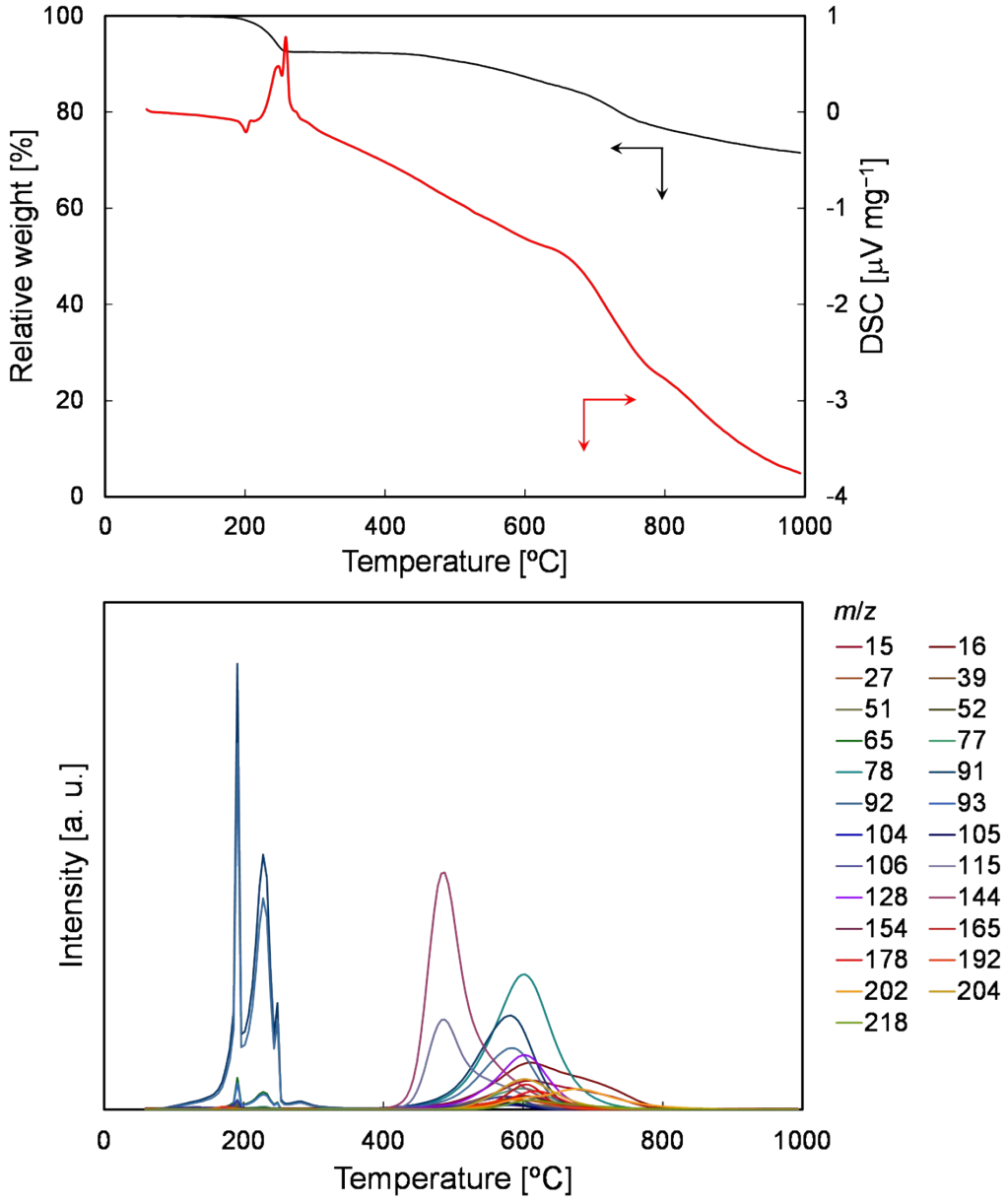

Figure S8. TG-DSC-MS profiles of TF*R*.

Decomposition of TF*S*

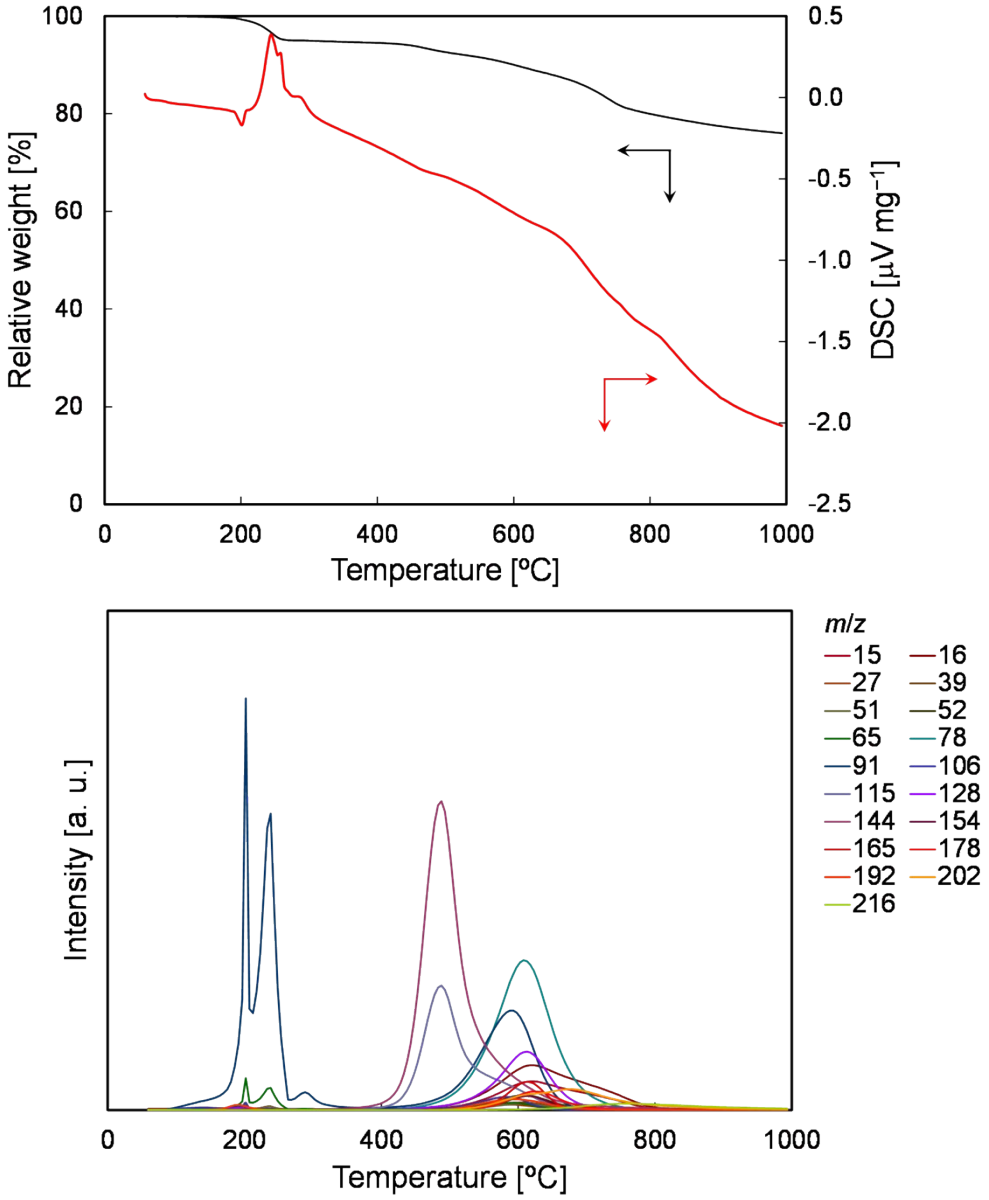

Figure S9. TG-DSC-MS profiles of TF*S*.

Raman spectra

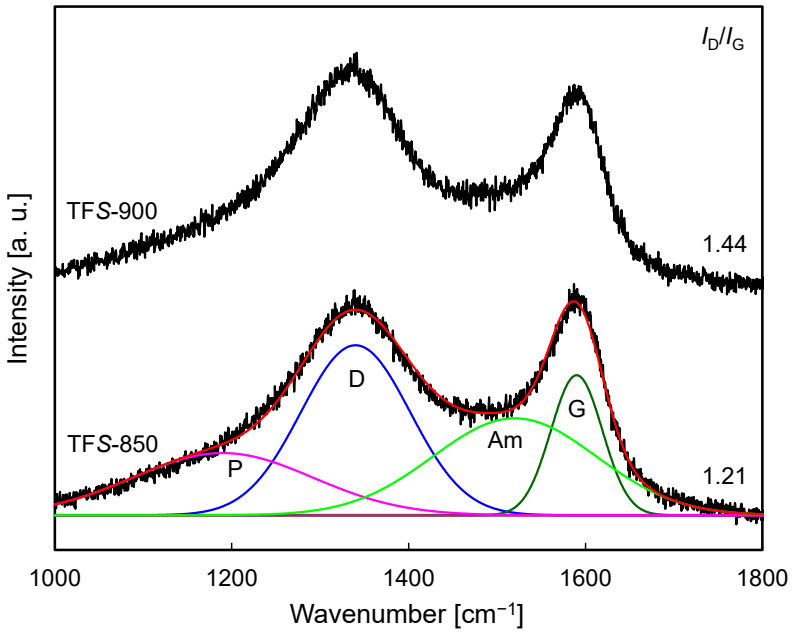

Figure S10. Raman spectra of TF*S*-850 and -900 formed on silica plates. The spectra are deconvoluted into four components: graphitic peak (G peak) at 1600–1580 cm^{-1}, disorder peak (D peak) at 1355–1340 cm^{-1}, a peak ascribed to amorphous carbon phase (Am peak) at 1525–1490 cm^{-1}, and a peak ascribed to sp^3-bonded carbon atoms (P peak) at 1190–1150 cm^{-1}.[S1,S2] The ratios of the peak areas are listed below in Table S1. The ratios of the intensities of the D peak to the G peak (I_D/I_G) are also shown in the figure. Both spectra are those typically observed for amorphous carbon and similar except for the increase in the I_D/I_G value with an increase in the heat treatment temperature, which is often observed for amorphous carbon.[S3–5] It should be noted that the absence of the peak attributed to C_{60} in the spectrum of TF*S*-850 might be due to the limited amount of C_{60} embedded only on the inner surface of the hollow-needle-like nanocarbon.

Table S1. Ratios [%] of deconvoluted peak area for Raman spectra of TF*S*-850 and -900.

	G	D	Am	P
TF*S*-850	14.0	34.9	30.5	20.6
TF*S*-900	12.2	37.4	29.6	20.8

Line defect on C_{60} crystal nanorod surface as a potential chiral alignment

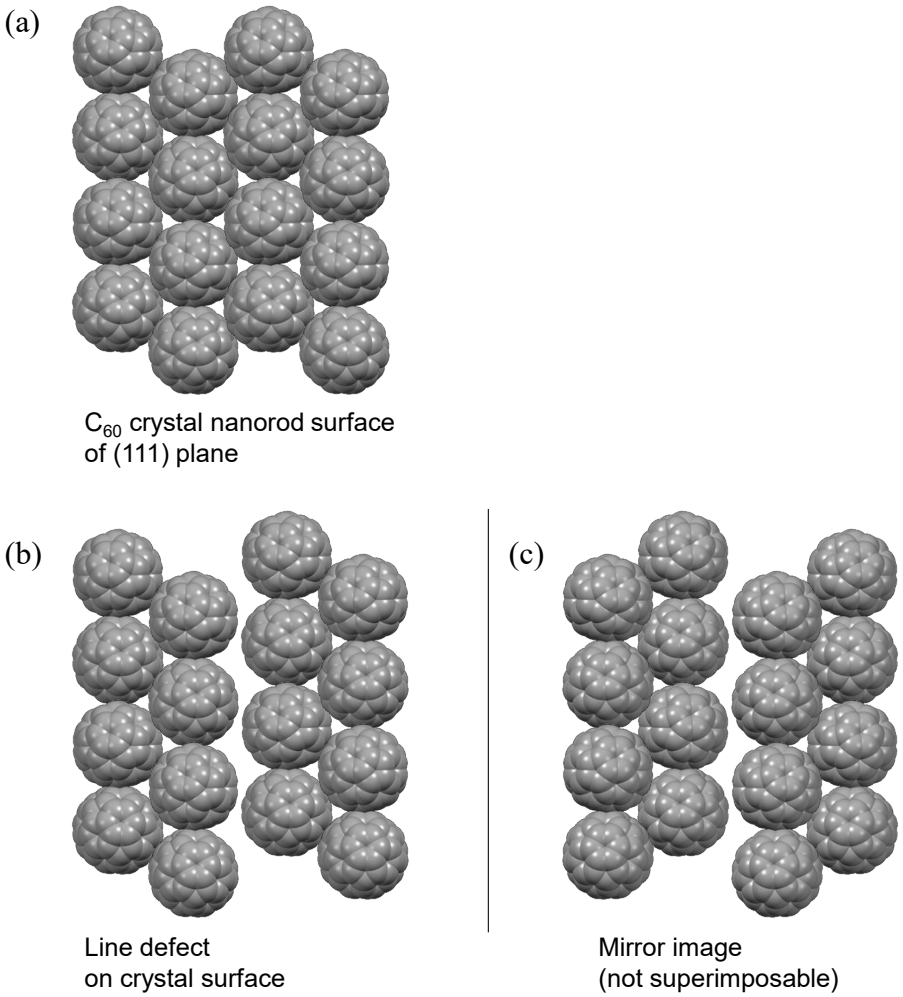

Figure S11. C_{60} alignments of (a) (111) plane of C_{60} crystal surface (b) that with line defect generated by gap and shift, and (c) its mirror image.

Stable configuration of BINOL on model of line defect of C60 crystal surface

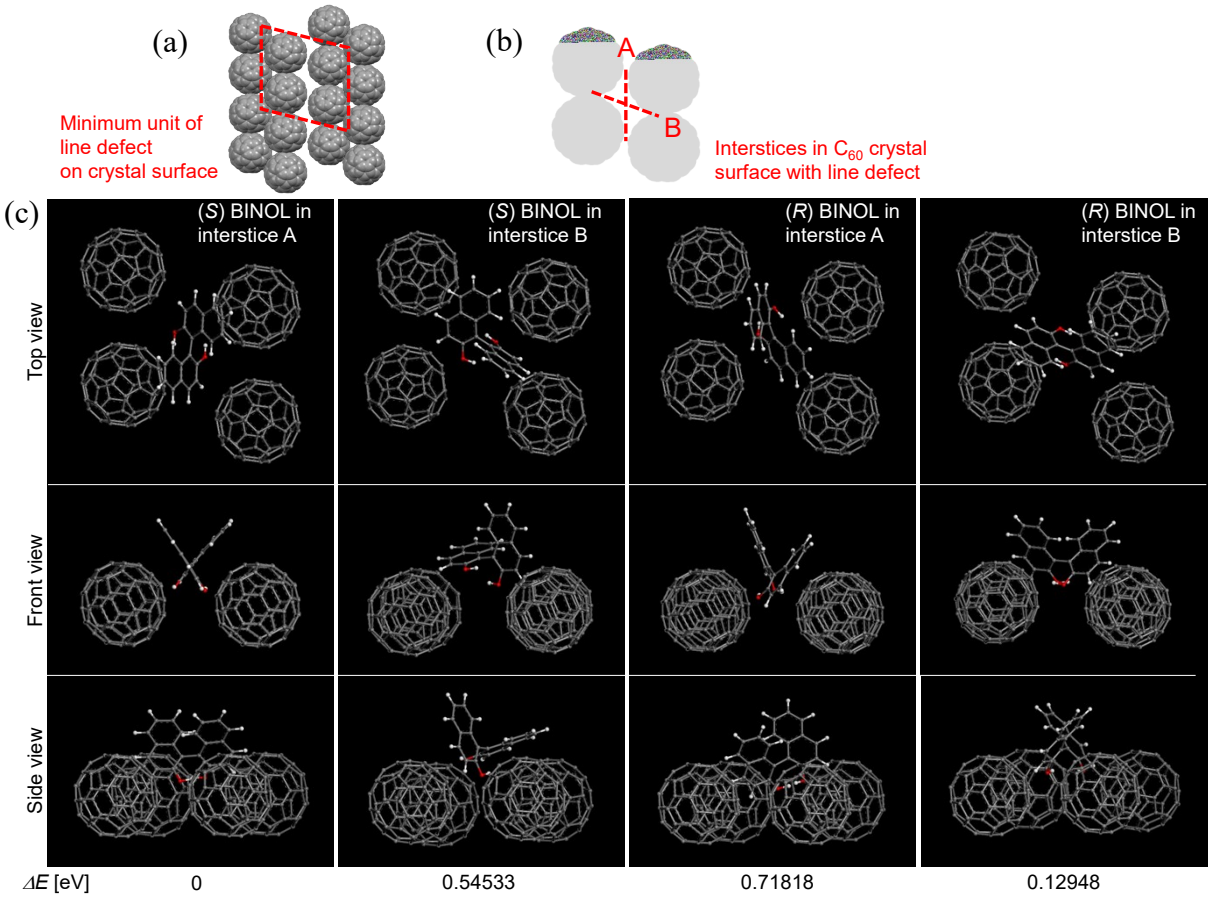

Figure S12. Schematic of (a) minimum unit of line defect on C_{60} crystal surface, (b) most probable two interstices that accommodate BINOL molecule, and (c) results of DFT calculations. The potential energy differences (ΔE) obtained by subtracting the energy for the combination of (*S*)-BINOL and the interstice A (the lowest energy, −273682.08144 eV) from those for the other combinations are shown. It should be noted that the most of the potential energy was derived from that for the four C_{60} molecules with the gap and the shift (−248638.98646 eV). The lowest energy obtained for (*S*)-BINOL indicates that the line defect model with the chiral surface C_{60} alignment have a higher affinity for (*S*)- than (*R*)-BINOL.

Chiral discrimination ability by alignment of C_{60} on inner wall surface

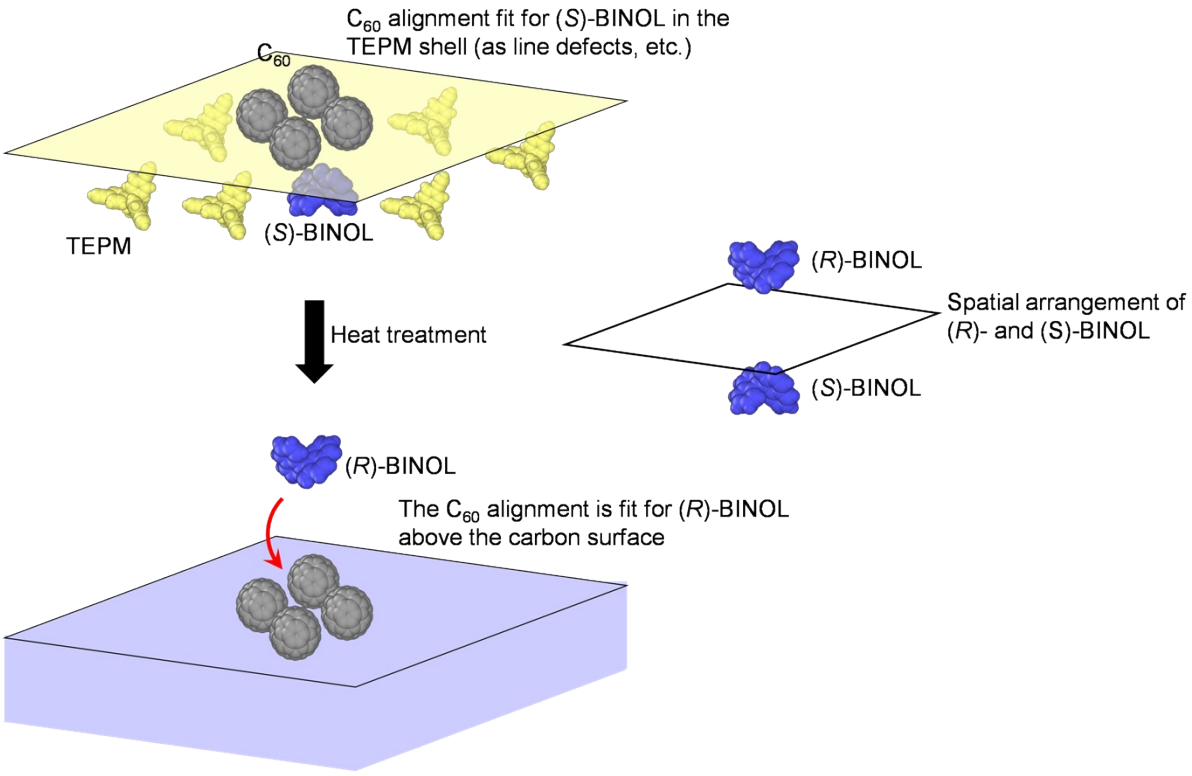

Figure S13. Schematic of alignment of C_{60} in precursor with TEPM, (*S*)-BINOL, and inner wall surface of carbon shell after heat treatment around 800–850 °C to remove C_{60} core by sublimation. In the upper figure, four C_{60} molecules are drawn as an example. The C_{60} core above the yellow plane is omitted for simplification.

CD spectra of hollow-needle-like nanocarbon

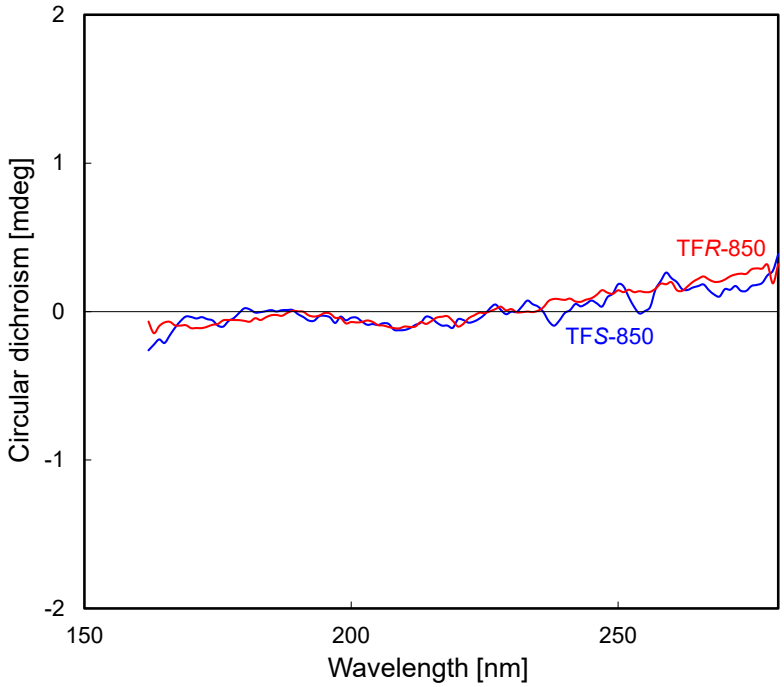

Figure S14. CD spectra of TF*R*- and TF*S*-850. The wavelength range was set according to our previous study.[16]

References

S1 A. Sadezky, H. Muckenhuber, H. Grothe, R. Niessner and U. Pöschl, *Carbon*, 2005, **43**, 1731−1742.

S2 F. Jaouen, F. Charreteur and J. P. Dodelet, *J. Electrochem. Soc.*, 2006, **153**, A689−A698.

S3 R. Yuan, Y. Guo, I. Gurgan, N. Siddique, Y. -S. Li, S. Jang, G. A. Noh and S. H. Kim, *Carbon*, 2025, **238**, 120214.

S4 T. Kaplas, A. Matikainen, T. Nuutinen, S. Suvanto, P. Vahimaa and Y. Svirko, *Sci. Rep.*, 2017, **7**, 8561.

S5 I. Karacan and L. Erzurumluoğlu, *Fibers Polym.*, 2015, **16**, 961–974.